A Theoretical Analysis of the Impact of Atmospheric Parameters on the Spectral, Electrical and Thermal Performance of a Concentrating III-V Triple-Junction Solar Cell

Marios Theristis[1,2,*], Eduardo F. Fernández[2], Cameron Stark[3], and Tadhg S. O'Donovan[1]

[1] Institute of Mechanical, Process and Energy Engineering, Heriot-Watt University, Edinburgh, EH14 4AS, UK

[2] Centro de Estudios Avanzados en Energía y Medio Ambiente (CEAEMA), University of Jaen, Campus las Lagunillas, Jaén 23071, Spain

[3] Center for Sustainable Energy Systems, Fraunhofer USA, Albuquerque, New Mexico, 87106, USA

*corresponding author email: mt208@hw.ac.uk

Abstract — The spectral sensitivity of a concentrating triple-junction (3J) solar cell has been investigated. The atmospheric parameters such as the air mass (AM), aerosol optical depth (AOD) and precipitable water (PW) change the distribution of the solar spectrum in a way that the spectral, electrical and thermal performance of a 3J solar cell is affected. In this paper, the influence of the spectral changes on the performance of each subcell and whole cell has been analysed. It has been shown that increasing the AM and AOD have a negative impact on the spectral and electrical performance of 3J solar cells while increasing the PW has a positive effect, although, to a lesser degree. A three-dimensional finite element analysis model is used to quantify the effect of each atmospheric parameter on the thermal performance for a range of heat transfer coefficients from the back-plate to the ambient air and also ambient temperature. It is shown that a heat transfer coefficient greater than 1300 W/(m^{2}K) is required to keep the solar cell under 100°C at all times. In order to get a more realistic assessment and also to investigate the effect of heat transfer coefficient on the annual energy yield, the methodology is applied for four US locations using data from a typical meteorological year (TMY3).

Keywords — concentrating photovoltaic (CPV), III-V multijunction solar cells, integrated modelling, spectral dependence, cooling requirements, electrical performance

1. Introduction

High Concentrating Photovoltaic (HCPV) systems use refractive or reflective optics to concentrate sunlight onto a smaller area made of high efficiency multijunction (MJ) solar cells. Such solar cells are made of III-V compound semiconductors and are used in both space and terrestrial applications [1]. Currently triple-junction (3J) solar cells made of GaInP/GaInAs/Ge are available in the market with an efficiency of up to 42% [2]. The subcells which consist a 3J solar cell are connected in series in a way to absorb a larger proportion of the spectral irradiance and thus, to achieve higher conversion efficiencies compared to the single junction cells [3]. However, the in-series connection and the different energy band-gap of each subcell cause a high spectral sensitivity. It is therefore necessary to model the effect of changing spectrum on the spectral, electrical and thermal performance of such devices. The HCPV performance is predominantly affected by the incident direct normal irradiance (DNI) [4] which in turn, is mainly determined by cloud cover [5], but also by changes in spectrum by variations of air mass (AM), aerosol optical depth (AOD) and precipitable water (PW).

HCPV modules can be either rated indoors and outdoors [6] under Concentrator Standard Test Conditions (CSTC, i.e. AM1.5D, DNI = 1000 W/m^2 and cell temperature T_{cell} = 25°C) or outdoors under Concentrator Standard Operating Conditions (CSOC, i.e. AM1.5D, DNI = 900 W/m^2, ambient temperature T_{amb} = 20°C and wind speed W_S = 2 m/s). The spectral conditions during the CSOC or outdoor I-V measurements for translation to CSTC [6] vary significantly compared to the standard ratings depending on the location and time of year because of the different atmospheric characteristics [7]. According to Muller et al. [6], the spectral filtering criteria have not yet been agreed within the International Electrotechnical

Commission (IEC). It is important therefore, to develop models or methods to identify the effects of each atmospheric parameter on the spectral and hence, the electrical and thermal performance of HCPV systems. Integrated modelling is necessary to enable the quantification of the spectral mismatch that will decrease the solar cell's electrical conversion efficiency resulting in an increase in heat, hence higher operating temperatures which will further reduce the electrical efficiency [8].

The majority of the commercial HCPV systems use refractive optics and passive cooling (e.g. Suncore [9] and Semprius [10]). The passive heat exchangers can be different in terms of their area and geometry depending on the application [11]. In order to achieve a T_{cell} below safe operating limits and to avoid long-term reliability issues, the incident DNI needs to be quantified because it is the dominant factor which contributes to the heat power production. Due to the MJ solar cell's spectral sensitivity, analytical modelling is required to estimate the cooling requirements taking into consideration the ambient and atmospheric conditions. Moreover, although the temperature dependence of MJ solar cells is lower than silicon cells [12, 13], it is crucial to design a robust cooling device to avoid elevated temperatures and therefore possible degradation issues or even the cause of fire [14, 15]. Oversizing the heat exchanger however will result in increasing the system's cost needlessly. Hence, a trade-off between reliability and cost must be achieved.

This work focuses on the accurate quantification of heat and therefore the cooling requirements using the heat transfer coefficient, h_{conv} (or the inverse thermal resistance R_{th}) from the back-plate of the concentrator cell assembly (CCA) to the ambient air as a criterion. It extends on a study introduced by Theristis and O'Donovan [16] where the impact of solar geometry (air mass) on the electrical and thermal performance of 3J solar cells was investigated. The same model is used here to assess the effect of AM, AOD and PW on the spectral, electrical and thermal behaviour of 3J solar cells. The modelling procedure and methodology are presented in section 2 and the results are analysed in section 3. In subsections 2.1 and 3.1, the effect of AM, AOD (at 500 nm) and PW on the spectral and electrical performance of a 3J solar cell is investigated at a subcell level but also as a whole device. In subsections 2.2 and 3.2, typical meteorological year (TMY3) [17] data of four US locations are used in order to investigate the spectral and electrical performance and also the effect of h_{conv} on the annual energy yield. TMY3 data are useful for the assessment of the electrical performance of CPV systems and for this work in particular, it can offer an estimate of the operating cell temperature and annual energy yield. However, since these data are typical, they do not offer a real representation of the system's operation under extreme conditions (i.e. worst-case scenarios) [17]. Therefore, in order to be able to quantify the cooling requirements under extreme conditions, a more suitable analysis is followed, in subsections 2.3 and 3.3, where the h_{conv} is quantified based on extreme heat generation within the solar cell (i.e. clear-sky, low AM, AOD, PW and high T_{amb}) and is compared with the h_{conv} based on the reference conditions of ASTM G173-03 [18] (AM1.5D, AOD = 0.084, PW = 1.42 cm). This study models the effects on the single cell level so the influence of other losses which can occur within a module can be avoided. Preliminary results have been published by Theristis et al. [19] however, an extended analysis is presented here incorporating individual subcell's performance along with additional case studies that enable the evaluation of the impact of each atmospheric parameter.

2. Modelling procedure

Three models are integrated: the spectral irradiance is generated by the NREL Simple Model of the Atmospheric Radiative Transfer of Sunshine, version 2 (SMARTS2) [20], an Electrical Model (EM) uses a single diode model to simulate the electrical characteristics and heat power of a 3J solar cell at Maximum Power Point (MPP) and a 3D Finite Element analysis Thermal Model (FETM) uses the heat power as an input from the electrical model in order to predict the temperature and the cooling requirements. The equations used for the EM and FETM models are presented by Theristis and O'Donovan [16, 21].

The spectral performance is evaluated using the spectral factor (SF) and spectral matching (or mismatch) ratio (SMR) as criteria; both of these spectral indices have been widely used in the PV community [22-25]. The SF of each subcell is given by [26]:

$$SF_i = \frac{\int DNI(\lambda)\cdot\eta_{opt}(\lambda)\cdot SR_i(\lambda)\,d\lambda}{\int DNI(\lambda)\,d\lambda}\cdot\frac{\int DNI_{ref}(\lambda)\,d\lambda}{\int DNI_{ref}(\lambda)\cdot\eta_{opt}(\lambda)\cdot SR_i(\lambda)\,d\lambda} = \frac{J_{sc}^{i}}{DNI}\cdot\frac{DNI_{ref}}{J_{sc,ref}^{i}} \quad (1)$$

while the SF of the whole device, due to the in-series connection, is given by:

$$\begin{aligned} SF &= \frac{\min\left(\int DNI(\lambda)\cdot\eta_{opt}(\lambda)\cdot SR_i(\lambda)\,d\lambda\right)}{\int DNI(\lambda)\,d\lambda}\cdot\frac{\int DNI_{ref}(\lambda)\,d\lambda}{\min\left(\int DNI_{ref}(\lambda)\cdot\eta_{opt}(\lambda)\cdot SR_i(\lambda)\,d\lambda\right)} \Rightarrow \\ SF &= \frac{\min\left(J_{sc}^{i}\right)}{DNI}\cdot\frac{DNI_{ref}}{\min\left(J_{sc,ref}^{i}\right)} \end{aligned} \quad (2)$$

where DNI(λ) is the incident spectral direct normal irradiance, $\eta_{opt}(\lambda)$ is the spectral optical efficiency, SR(λ) is the spectral response and J_{sc} is the short-circuit current density. The subscript, “ref”, denotes the reference conditions and “i” the corresponding subcell (1 = top, 2 = middle, 3 = bottom). SF values above 1 indicate spectral gains, below 1 indicate spectral losses and equal to 1 the same spectral conditions as the reference. The output current of the 3J solar cell is restricted to the minimum current of the three subcells because of the in-series connection.

On the other hand, the SMR of top to middle subcell is described as [27-29]:

$$SMR = \frac{\dfrac{\int DNI(\lambda)\cdot\eta_{opt}(\lambda)\cdot SR_{top}(\lambda)\,d\lambda}{\int DNI_{ref}(\lambda)\cdot\eta_{opt}(\lambda)\cdot SR_{top}(\lambda)\,d\lambda}}{\dfrac{\int DNI(\lambda)\cdot\eta_{opt}(\lambda)\cdot SR_{middle}(\lambda)\,d\lambda}{\int DNI_{ref}(\lambda)\cdot\eta_{opt}(\lambda)\cdot SR_{middle}(\lambda)\,d\lambda}} = \frac{\dfrac{J_{sc}^{top}}{J_{sc,ref}^{top}}}{\dfrac{J_{sc}^{mid}}{J_{sc,ref}^{mid}}} \tag{3}$$

where SMR > 1 when the incident spectrum is blue rich and SMR < 1 when the incident spectrum is red rich. The SMR = 1 when the incident spectrum matches the reference conditions.

2.1. Impact of atmospheric parameters on spectral and electrical performance

Firstly, the impact of AM, AOD and PW on the spectral and electrical performance of a triple-junction solar cell has been investigated for a given cell temperature. In order to achieve this, an algorithm was developed to vary each parameter while keeping all others constant at the reference conditions of ASTM G173-03 [18].

2.2. Case studies using TMY3 data and regression analysis

Case studies have been performed to determine the spectral and electrical performance and also to quantify the optimum h_{conv} at four USA locations with relatively high annual direct normal irradiation; Albuquerque (New Mexico), El Paso (Texas), Las Vegas (Nevada) and Tucson (Arizona). A method has been developed to generate bulk spectra [19, 30] using atmospheric data from a TMY3. It is worth mentioning that the use of high-quality observed data of the main atmospheric parameters in conjunction with the SMARTS2 model has been widely used by the scientific community and proven to be valid for the evaluation of HCPV and PV performance [31-34]. To ensure clear-sky conditions, the spectral global normal irradiance GNI(λ) generated by SMARTS2 was integrated over the whole range of wavelengths and a filter has been applied on TMY3 for DNI/GNI > 0.8. This filter is also included in the draft of

IEC 62670-3 [6]. Furthermore, to avoid high computational time, regression analysis has been used to predict the T_{cell} as a function of P_{heat}, T_{amb} and h_{conv}.

2.3. Quantification of cooling requirements

In order to quantify the CCA's cooling requirements (or h_{conv}) under extreme conditions, the EM and FETM have been simulated iteratively for given solar spectra generated in SMARTS2. HCPV cooling requirements should be designed for AM < 1.5 because of the current mismatch between the top and middle subcells, which subsequently contributes to greater heat, and also because of the higher irradiance intensity [16]. Assuming an initial temperature $T_{cell}(s) = 25°C$ (where "s" is the number of state), the EM ran the single diode model which calculated the electrical characteristics and hence, the heat generated within the solar cell by [35]:

$$P_{heat} = (CR \cdot DNI \cdot A \cdot \eta_{opt}) \cdot (1 - \eta_{cell}) \quad (4)$$

where CR is the concentration ratio, A is the area of the solar cell, η_{opt} is the optical efficiency and η_{cell} is the electrical conversion efficiency. The heat power was then imported to the FETM as a boundary condition on the solar cell's surface to model it as a heat source and hence, to predict the temperature distribution. The predicted volumetric solar cell temperature was then imported back to the EM and the integrated models ran iteratively until a steady state was reached between them i.e. when $|T_{cell}(s+1)-T_{cell}(s)| \leq 0.002°C$.

3. Results and analysis

The CCA used for this study is the C1MJ from Spectrolab [36] and the External Quantum Efficiency (EQE) data at 25°C, 45°C, 65°C and 75°C were taken from Kinsey and Edmondson [37]. The results below correspond to a CR = 500× and an η_{opt} = 80%. All the inputs and boundary conditions to the EM and FETM are similar to those presented by Theristis and O'Donovan [16] unless otherwise stated.

3.1. Impact of individual atmospheric parameters on spectral and electrical performance

This section assesses the impact of individual atmospheric parameters (AM, AOD, PW) on the spectral and electrical performance of the Spectrolab C1MJ CCA at 25°C. Realistic ranges were selected ($1 \leq AM \leq 10$, $0 \leq AOD \leq 1$, $0\ cm \leq PW \leq 5\ cm$) for each atmospheric parameter. Although a similar approach has been reported by Fernández et al. [26] (using only the whole cell's SF as a criterion), it is also presented here in order to get a better understanding of which (and to what extent) parameters contribute to the heat generated on the CCA and therefore the cooling requirements and electrical energy performance of such devices for a range of conditions. For this reason, it is necessary to model the SF (whole cell and individual subcell), normalised electrical power ($P_{el,norm}$) and normalised heat power ($P_{heat,norm}$) as a function of each atmospheric parameter by varying each one (from low to high values) at a time while keeping the rest at the reference conditions of ASTM G173-03 as previously considered [26, 38, 39].

3.1.1. Impact of air mass

Fig. 1 (left) shows the impact of AM on the spectral DNI distribution. The significant drop of the spectral intensity is obvious with increasing AM. It can also be noticed that there is a shift toward the longer wavelengths. The impact of changing spectrum due to variation of AM on the electrical performance is also shown in Fig. 1 (right); the SF1 of the top subcell shows spectral gains up to 2.1% for AM < 1.5 while the middle (SF2) and bottom (SF3) subcells show the opposite behaviour (-3.7% (middle subcell), -3% (bottom subcell) losses for AM < 1.5 and gains for AM > 1.5). The whole solar cell's spectral factor (SF) follows the top subcell for AM > 1.5 while is close to SF2 for AM < 1.5. The reason for this is that at CSTC conditions the middle subcell limits the current by a 1.6% difference from the top's current. Furthermore,

Fig. 1 (right) shows the impact of AM on the $P_{el,norm}$ and $P_{heat,norm}$; the $P_{el,norm}$ losses are ≤ 1% up to AM1.9D while for AM > 2 the losses increase significantly (6.7% at AM3D, 20.1% at AM5D and 50.3% at AM10D). The $P_{heat,norm}$ increases with the excess current mismatch (4.1% at AM3D, 12.2% at AM5D and 30.4% at AM10D) and therefore it is always greater than 0% except when the top and middle subcells are current matched; i.e. when it operates at the reference conditions. Only the AM values up to AM = 3 have been illustrated in Fig. 1 (right) for clarity purposes and also due to the significantly higher solar intensity, which in turn affects the thermal performance and cooling requirements of HCPV systems. Moreover, low AM values predominantly occur during the summer months at locations with a high annual direct solar irradiation.

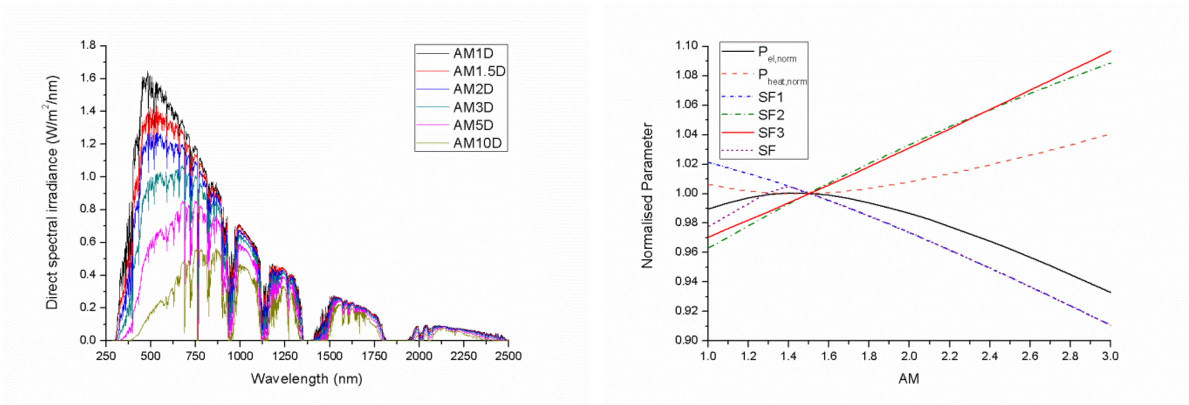

Fig. 1. Effect of AM on the spectral irradiance (left figure) with the rest of the parameters kept constant according to the ASTMG173-03 [18]. The figure on the right shows the impact of AM on the spectral and electrical performance of C1MJ CCA.

3.1.2. Impact of aerosol optical depth

Increasing AOD reduces the spectral irradiance in the short wavelengths region (visible light) and to a much lesser degree in the near-infrared light (Fig. 2 left); this will have a significant influence on the current generation of the top subcell. From Fig. 2 (right) it can be seen that the middle subcell is almost unaffected by AOD (maximum losses of 1% on SF2) while the top subcell shows losses of up to 36.3% at AOD = 1. However, for AOD lower than the reference value (AOD_{ref} = 0.084) the SF1 shows spectral gains up to 3.5%. SF3 has the opposite trend from SF1; spectral losses are down by 3.95% for AOD below reference conditions and gains up by 40.86% for AOD > 0.084. The SF for the whole solar cell shows the same behaviour as in the variable AM following the SF1 for values higher than the reference, since the limiting subcell is the top one. The effect of the current mismatch which was just described is evident when the $P_{heat,norm}$ and $P_{el,norm}$ are assessed; when the current mismatch between the subcells increases, the $P_{heat,norm}$ increases by up to 21.1% while the $P_{el,norm}$ is reduced by 34.9% when AOD is equal to 1.

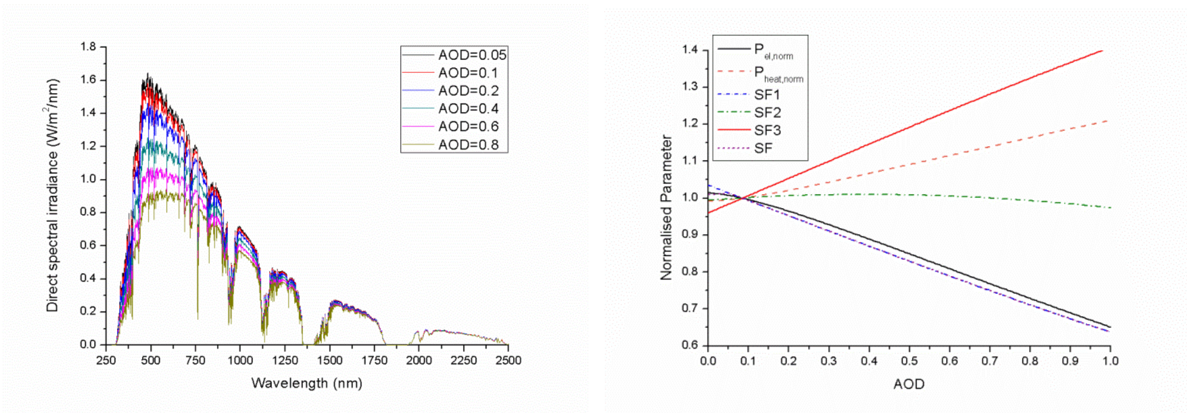

Fig. 2. Effect of AOD on the spectral irradiance (left). The rest of the parameters are kept constant according to the ASTMG173-03. On the right figure, the impact of variable AOD on the spectral and electrical characteristics is shown.

3.1.3. Impact of precipitable water

In a similar manner to section 3.1.1. and 3.1.2., Fig. 3 (left) shows the impact of PW on the spectral DNI; in contrast to AOD, increasing PW has a minimal effect in the short wavelengths, however the longer wavelengths show a reduction. Hence, the bottom subcell, that corresponds to the infrared region will have higher spectral losses with increasing PW. The middle subcell which converts the near-infrared region will also be affected but to a lesser extent. As can be seen from Fig. 3 (right), for PW values lower than 1.42 cm (reference conditions), SF1, SF2 and hence, SF show losses due to the current mismatch between the top (-14.6%) and middle (-11.5%) subcells, however the SF3 shows gains of up to 21.1% and therefore increases in $P_{heat,norm}$ occur up to 7.8% with a significant drop (12.9%) in $P_{el,norm}$. For PW values higher than 1.42 cm, the drop in the infrared region causes significant losses (down by 10.2%) on the bottom subcell which corresponds to the infrared proportion of the solar spectrum, hence a higher performance is noticed with $P_{el,norm}$ and SF gains up to 4.3%. This is due to the significant reduction of the excess current of the germanium subcell, therefore lower $P_{heat,norm}$ by 2.6% at PW = 5 cm and a higher electrical conversion efficiency.

Overall, as discussed also by Fernández et al. [26], the dominant atmospheric parameters that affect the performance of 3J solar cells are the AM and AOD with losses on the $P_{el,norm}$ down by 50.3% at AM10D and 34.9% at AOD = 1.

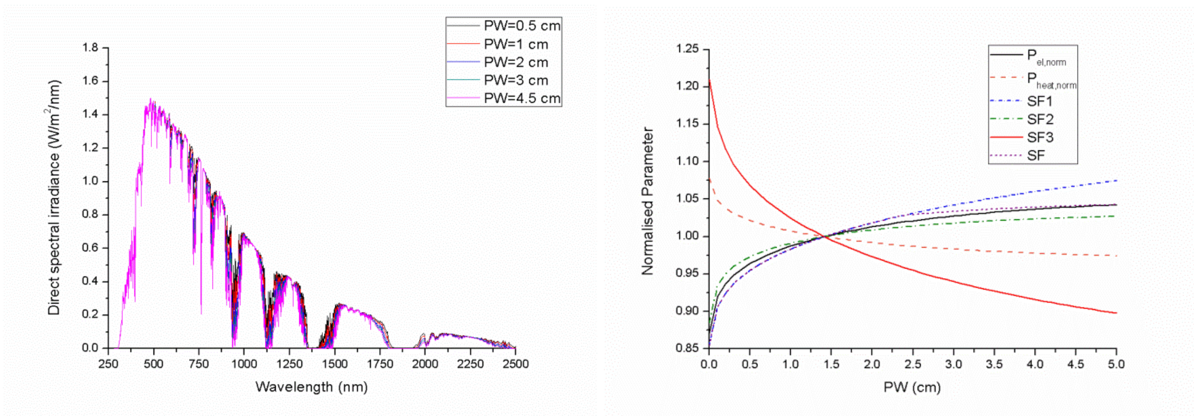

Fig. 3. Effect of PW on the spectral irradiance (left). The rest of the parameters are kept constant according to the ASTMG173-03. On the right figure, the impact of variable PW on the spectral and electrical characteristics is shown.

3.2. Case Studies

Locations offering relatively high annual direct solar irradiation and hence applicable for CPV applications were selected to investigate the effect of the heat transfer coefficient on temperature and therefore, the electrical power production. Class I TMY3 hourly data have been used for four locations in the USA (Albuquerque, El Paso, Las Vegas and Tucson). The location characteristics are shown in Table I.

Table I: Sites used for the simulation along with the coordinates and elevation

Location	**Latitude**	**Longitude**	**Elevation (m)**
Albuquerque	35.04°N	106.62°W	1619
El Paso	31.77°N	106.50°W	1186
Las Vegas	36.08°N	115.15°W	648
Tucson	32.13°N	110.95°W	777

The filtering criterion resulted in 3089 hourly spectra for Albuquerque, 3180 for El Paso, 3320 for Las Vegas and 3300 for Tucson. Monthly average values of the filtered data are illustrated below in Fig. 4 for all the locations.

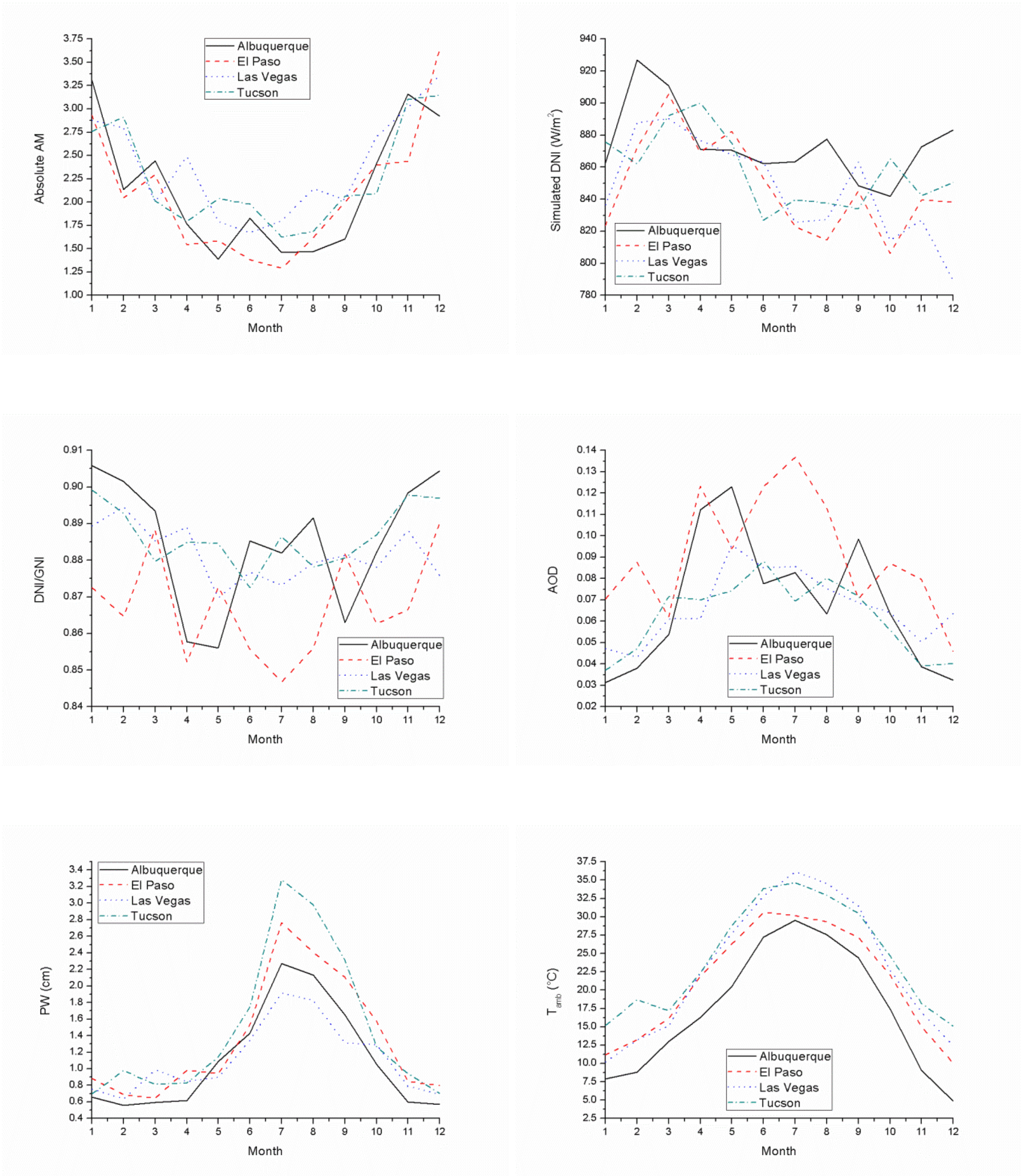

Fig. 4. Monthly average values of filtered data for all locations; a) absolute air mass, b) simulated direct normal irradiance (DNI), c) clearness ratio (DNI/GNI), d) aerosol optical depth (AOD), e) precipitable water (PW) and f) ambient temperature (T_{amb}).

Due to the high volume of data (>11.5x10^6 lines of generated spectra in addition to the TMY3 data), regression analysis has been performed for the calculation of cell temperature. Initially a parametric study was simulated in the FETM for 20 W ≤ P_{heat} ≤ 30 W, 1200 W/(m^2K) ≤ h_{conv} ≤ 1600 W/(m^2K), 15°C ≤ T_{amb} ≤ 45°C and the cell temperature could then be calculated using the following equation:

$$T_{cell} = \alpha + \beta \cdot P_{heat} + \gamma \cdot h_{conv} + \delta \cdot T_{amb} \tag{5}$$

where the intercept and linear coefficients are α = 35.12°C, β = 1.80°C/W, γ = -0.02°C/(W$m^{-2}K^{-1}$), δ = 1.00. The R^2 between modelled (in FETM) and predicted (regression) data was 0.9975 (Fig. 5). It is important to mention that the effect of W_S was not taken into consideration in equation (5) however, experimental results have proven that the effect of W_S on the estimation of T_{cell} is low, and therefore it can be neglected in a first approximation [40].

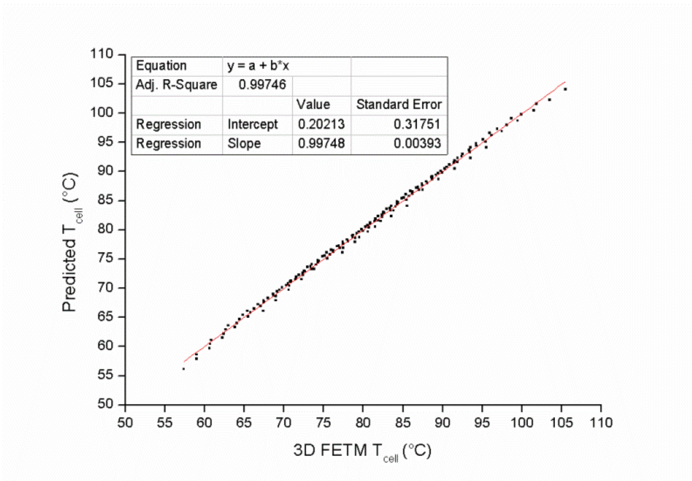

Fig. 5. Linear regression analysis of T_{cell} between simulated (in 3D FETM) and predicted data for the C1MJ solar cell.

As mentioned in Section 2, the normalised short-circuit current or SF is a useful index to evaluate the spectral performance of a solar cell; Fig. 6a illustrates the SF for all locations. It can be seen that spectral gains occur in July and August for Albuquerque (0.6% and 1% respectively) and Tucson (1.7% and 1.6% respectively) while El Paso shows spectral gains only occur in July (1.9%). Las Vegas has spectral losses during all months of the year with the lowest during December (a decrease of 12.2%). The SMR follows a similar trend to SF in Fig. 6b and this is because both parameters are a function of the short-circuit current; the top subcell seems to be the current limiter for the whole year except when SF is above 1. This indicates that spectral gains occur when the incident spectrum is blue rich.

In Fig. 6c and 6d the normalised heat and electrical powers are shown respectively where, as expected, they exhibit the opposite behaviour. All locations show $P_{el,norm}$ losses all year round (as compared to the reference conditions) and therefore the $P_{heat,norm}$ shows gains; this is another indication that AM1.5D is not an appropriate reference for the cooling requirements estimation [16].

Finally, as expected, the calculated T_{cell} (Fig. 6e) peaks during the summer months for all locations; this is mainly due to the higher ambient temperatures. The monthly averages show temperatures of up to 88°C which are relatively high, if long term degradation issues are considered [41]. The heat generated on the solar cell is mainly influenced by the system's characteristics (i.e. CR, A, η_{opt}), the electrical conversion efficiency and of course the incident DNI which in turn, is affected by the changes in the solar spectrum (i.e. AM, AOD, PW, etc) (equation (4)). The P_{heat}, h_{conv} and T_{amb} are the parameters affecting the T_{cell} (equation (5)). Since the cooling mechanism for all locations is assumed to be the same, the cell temperature difference between locations is dependent on P_{heat} and T_{amb}. Tucson exhibits the highest T_{cell} during the year except the months from June to September where the T_{cell} is higher in Las Vegas. When Las Vegas and Tucson are compared, it can be noticed that the T_{cell} follows the trend of T_{amb} except in June where although the T_{amb} is higher in Tucson, the T_{cell} is higher in Las Vegas by 1°C. This can be attributed to the higher DNI in Las Vegas (by 4.2%) in combination with the higher PW (by 29.9%) in Tucson, which limits the excess current on the bottom subcell and therefore contributes to the heat reduction. In July, August and September the T_{amb} is higher in Las Vegas (by 1.5°C, 1.6°C and 1°C respectively) and also the PW values are much higher in Tucson (by 71.6% in July, 63.3% in August and 76.8% in September) and therefore the T_{cell} is higher in Las Vegas by 1.3°C, 1.8°C and 3°C. Although Albuquerque exhibits higher DNI than El Paso during the year (except in May), it shows the lowest T_{cell} (except in July and August) due to the lower T_{amb}. In July, the monthly average T_{cell} in Albuquerque is 1.6°C higher than El Paso due to lower T_{amb} difference (0.64°C) between them and also due to the higher PW (by 0.5 cm or 17.8%) and AOD (by 39.6%) in El Paso. In August the SMR value for Albuquerque is 1.03 whereas for El Paso is 0.99; this indicates a clearer atmosphere (lower AOD values by 43.9%) in Albuquerque and therefore higher DNI and hence higher T_{cell} even if T_{amb} is lower by 1.78°C as compared to El Paso.

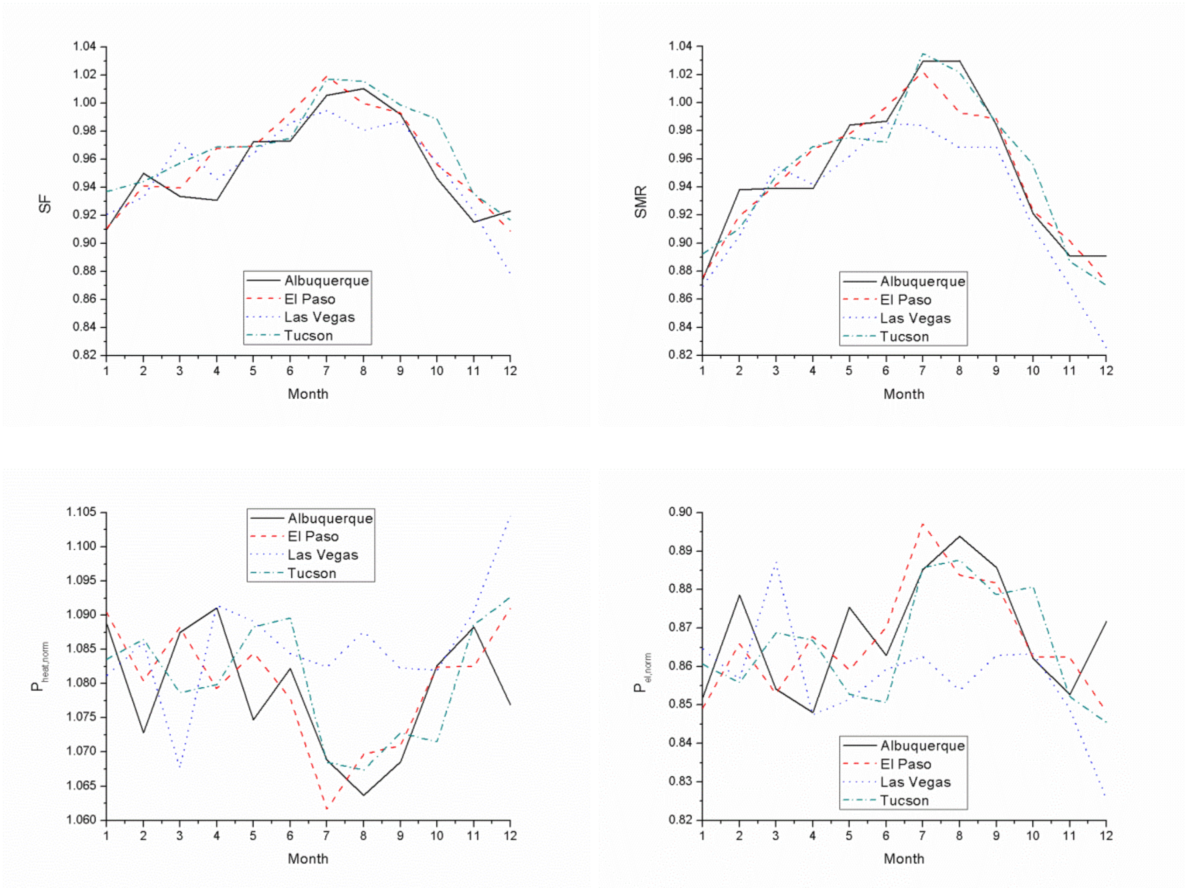

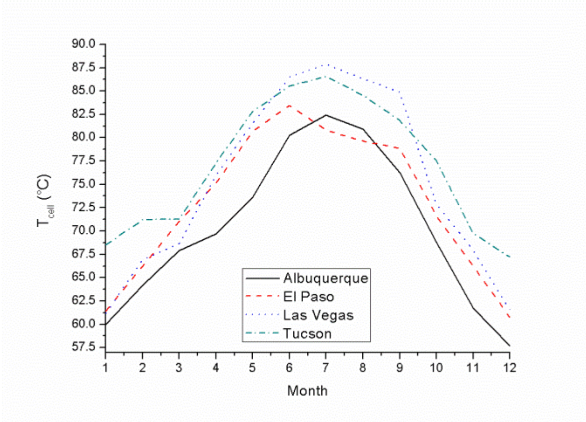

Fig. 6. Monthly average outputs of numerical model: a) spectral factor, b) spectral mismatch ratio, c) normalised heat power, d) normalised electrical power and e) solar cell temperature.

Annual average inputs and outputs for all locations can be seen in Table II and III respectively. Due to the relatively similar atmospheric inputs, all locations exhibit similar annual average outputs; the SF ranges from 0.95 to 0.97, the $P_{el,norm}$ from 0.86 to 0.87 and the $P_{heat,norm}$ from 1.08 to 1.09. The T_{cell} however, ranges from 70.3°C to 77°C and follows the trend of the T_{amb} inputs. Las Vegas has the highest spectral and electrical power losses of 5% and 14% respectively and the highest gains in $P_{heat,norm}$ of 9%, it exhibits the second highest annual average T_{cell}. The highest annual average T_{cell} of Tucson can be attributed to the higher annual average T_{amb} which is 1.37°C (5.6%) higher than the one in Las Vegas. Moreover, although the higher annual average PW in Tucson shows a relatively better SF (and hence lower heat) it is shown that the dominant parameter for this temperature difference between locations with similar location characteristics is influenced by the T_{amb}. This can also be noticed when Albuquerque and El Paso are compared; although the SF, $P_{el,norm}$ and $P_{heat,norm}$ values are the same, the annual average T_{cell} is 2.7°C higher in El Paso because of the higher T_{amb}.

Table II: Annual average inputs for all locations.

Location	DNI (W/m^2)	T_{amb} (°C)	AM_{abs}	AOD	PW (cm)
Albuquerque	874.25	17.21	2.16	0.07	1.10
El Paso	847.71	21.08	2.10	0.09	1.35
Las Vegas	847.37	22.97	2.39	0.07	1.11
Tucson	858.42	24.34	2.27	0.06	1.47

TABLE III: Annual average outputs for all locations.

Location	SF	$P_{el,norm}$	$P_{heat,norm}$	T_{cell} (°C)
Albuquerque	0.96	0.87	1.08	70.3
El Paso	0.96	0.87	1.08	73.0
Las Vegas	0.95	0.86	1.09	75.2
Tucson	0.97	0.87	1.08	77.0

Additional simulations were conducted in order to assess the impact of h_{conv} on the energy yield at each location using a range of h_{conv} within the passive cooling limits (i.e. 1000 W/(m^{2}K) ≤ h_{conv} ≤ 1600 W/(m^{2}K) with a step of 200 W/(m^{2}K)). The results are shown in Fig. 7 and Table IV for the following annual direct normal irradiation values: 2696 kWh/m^2 in Albuquerque, 2643 kWh/m^2 in El Paso, 2722.4 kWh/m^2 in Las Vegas and 2765.5 kWh/m^2 in Tucson.

Fig. 7 shows the annual E_{yield} in kWh/kWp as a function of h_{conv} for all the locations; as expected, the E_{yield} increases with the annual direct normal irradiation, since the DNI is the main driver for the energy output. The E_{yield} also increases linearly with h_{conv} with the slopes of the linear fit at 0.14 for Albuquerque and El Paso and 0.15 for Las Vegas and Tucson. Table IV shows the annual maximum T_{cell} for four values of h_{conv} and also the annual average T_{cell} in parenthesis. It can be seen that the cell temperature exceeds 100°C in Las Vegas and Tucson for h_{conv} = 1000 W/(m^{2}K). If the temperature limit is set at 90°C, the cooling requirements for Albuquerque and El Paso would be h_{conv} > 1250 W/(m^{2}K); for Las Vegas h_{conv} > 1450 W/(m^{2}K) and for Tucson a h_{conv} > 1350 W/(m^{2}K). The annual average T_{cell} reduction per W/(m^{2}K) increase is 0.027 for all four locations.

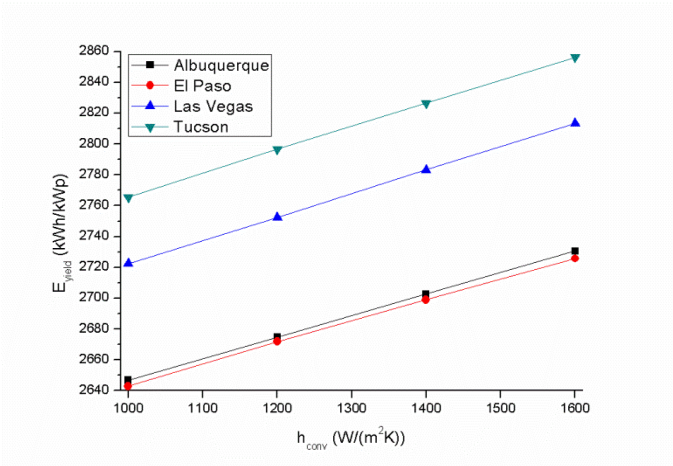

Fig. 7. Annual values of energy yield as a function of the heat transfer coefficient.

TABLE IV: Annual maximum and average (in parenthesis) T_{cell} as a function of h_{conv}.

Location	**h_{conv} (W/(m^{2}K))**			
	1000	1200	1400	1600
Albuquerque	96.5°C (71.4°C)	90.9°C (65.9°C)	85.4°C (60.5°C)	79.8°C (55°C)
El Paso	97.1°C (74.1°C)	91.5°C (68.6°C)	86°C (63.2°C)	80.4°C (57.7°C)
Las Vegas	102.5°C (77°C)	96.9°C (71.5°C)	91.4°C (66.1°C)	85.8°C (60.6°C)
Tucson	100°C (78°C)	94.5°C (72.5°C)	88.9°C (67.1°C)	83.3°C (61.6°C)

3.3. Cooling requirements under extreme conditions

As discussed in the introduction, the study conducted in section 3.2. using TMY3 data is useful for the electrical performance and operating temperature evaluation of CPV for a particular location. However, it may have the disadvantage of not allowing the accurate quantification of the cooling requirements under extreme conditions. Hence, this section evaluates the cooling requirements of the C1MJ CCA under worst-case scenarios. The AM is fixed to AM = 1 and the AOD and PW have been varied for specific ranges that would trigger relatively high thermal stresses on the CCA due to additional current mismatch between the subcells and also due to higher solar irradiance intensities. Moreover, in the summer months and for latitudes lower than 40°N, the AM is lower than AM = 2 for most of the day [42]. Therefore, AM1D is considered under variable AOD and PW, for the estimation of the required h_{conv} from the back plate to the ambient air with an ambient temperature of 45°C. Also, the ranges of AOD ($0.05 \leq AOD \leq 0.2$) and PW ($0.5 \leq PW \leq 1.5$ cm) were chosen to simulate the thermal behaviour of CCA at relatively hot (high T_{amb}), clear (low AOD) and dry (low PW) conditions. Any cooling device designed to dissipate heat under these conditions, will be adequate for higher AM, AOD and PW values. A range of heat transfer coefficients 1200 W/(m^{2}K) $\leq h_{conv} \leq$ 1600 W/(m^{2}K) are used as a boundary condition on the back surface of the CCA. Higher heat transfer coefficients were not considered in order to stay within passive cooling limits [43]. The cell's temperature is then predicted by the FETM and the integrated volumetric temperature is then imported back to the EM. The procedure is repeated until a steady state is reached between the EM and FETM; i.e. solar cell temperature difference lower than 0.002°C. The solutions converge in all cases after the 3rd iteration.

The temperature distribution of the C1MJ CCA is shown in Fig. 8 for AM1D, PW = 1.42 cm, AOD = 0.084, h_{conv} = 1600 W/(m^{2}K) (i.e. 1.22 K/W, area of 5.13x10^{-4} m^2) and T_{amb} = 45°C. A maximum temperature of 89.84°C is observed at the centre of the cell while the temperature of the top layer of the DBC board, which is not illuminated, varies from 70°C at the edges to 80°C near the cell. The integrated volumetric temperature of the solar cell is 86.34°C.

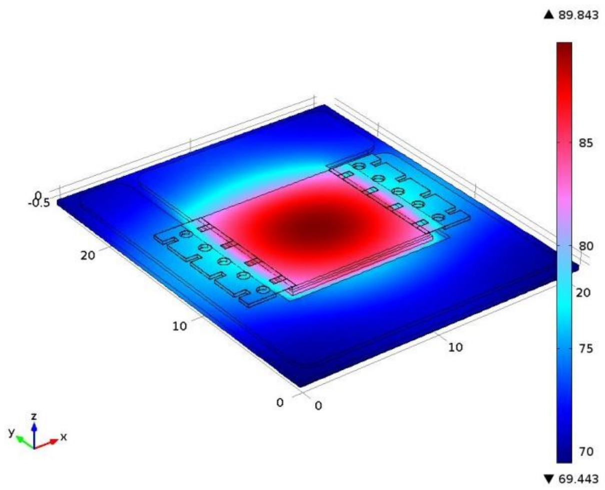

Fig. 8. Temperature distribution (°C) across the C1MJ CCA for AM1D, h_{conv} = 1600 W/(m^2K) and T_{amb} = 45°C.

The influence of the changing spectra on the calculated integrated volumetric cell temperatures are illustrated in Fig. 9 for AM1D, 0.05 ≤ AOD ≤ 0.2, 0.5 cm ≤ PW ≤ 1.5 cm, 1200 W/(m^2K) ≤ h_{conv} ≤ 1600 W/(m^2K) and T_{amb} = 45°C. The reference spectrum AM1.5D ASTM G173-03 is also plotted (black line) for comparison. As can be seen, cooling devices designed at AM1.5D will allow higher operating temperatures (by up to 9.3°C) at relatively "hot and dry" sites. The elevated temperatures will cause long term degradation problems if kept for a prolonged time [41]. Therefore, at sites with low AOD and PW, the h_{conv} should be higher than 1300 W/(m^2K) in order to operate at temperatures lower than 100°C.

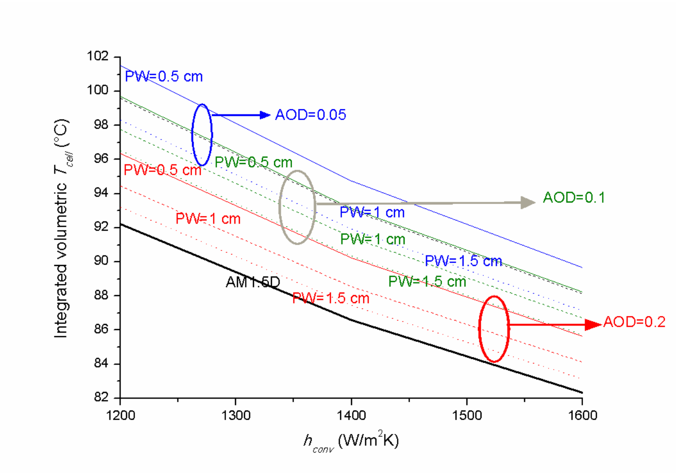

Fig. 9. Integrated volumetric solar cell temperature as a function of heat transfer coefficient, aerosol optical depth (blue AOD = 0.05, green AOD = 0.1, red AOD = 0.2) and precipitable water (straight lines PW = 0.5 cm, dash lines PW = 1 cm, dot lines PW = 1.5 cm). The air mass is kept constant at AM1D. The AM1.5D ASTM G173-03 is also shown with black colour.

4. Discussion and conclusion

An integrated modelling procedure has been presented in order to evaluate the impact of atmospheric parameters on the spectral, electrical and thermal performance of a concentrating III-V triple-junction solar cell under a CR of 500×. The results show that such solar cells are mainly influenced by changes in AM and AOD with spectral losses of 51.3% at AM10D and 36.3% when AOD = 1. The PW however showed spectral gains of up to 4.3% when PW = 5 cm; this is attributed to the reduction of the infrared portion of spectrum. Moreover, the $P_{el,norm}$ losses are < 1% up to AM1.9D while for AM values greater than AM2D the losses increase significantly (up to 50.3% at AM10D). The $P_{heat,norm}$ increases with the excess current mismatch between the subcells and therefore it is always greater than 0%, except when the top and middle subcells are current matched; i.e. when it operates at the reference conditions. Similarly with increasing AOD, the $P_{el,norm}$ is reduced by 34.9% when AOD = 1 while for PW = 5 cm it is increased by 4.3% and therefore the $P_{heat,norm}$ is decreased by 2.6%.

The procedure was simplified in order to handle bulk spectra. Instead of using the 3D FETM model, regression analysis has been performed for the calculation of T_{cell} using equation (5). Class I TMY3 data have been used for four US locations with relatively high annual DNI (Albuquerque, El Paso, Las Vegas and Tucson) in order to evaluate the performance of a CCA. It was shown that Las Vegas and Tucson exhibited the highest annual average spectral losses and T_{cell} respectively. $P_{el,norm}$ is always underperforming in Las Vegas while for Albuquerque and El Paso gains were visible for a $h_{conv} > 1200$ W/(m^{2}K); Tucson exhibited $P_{el,norm}$ gains for $h_{conv} \geq 1600$ W/(m^{2}K). By varying the h_{conv} at each location, its influence on E_{yield} could then be determined. Because the TMY3 represent average values, a stricter T_{cell} limit was assumed suggesting a different h_{conv} at each location; 1250 W/((m^{2}K)) for Albuquerque and El Paso, 1450 W/(m^{2}K) for Las Vegas and 1350 W/(m^{2}K) for Tucson.

Finally, a method was also presented in order to evaluate the cooling requirements under extreme conditions; i.e. AM1D, $T_{amb} = 45$°C and a relatively clear (low AOD) and dry (low PW) atmosphere. It has been shown that in order to operate at a maximum T_{cell} lower than 100°C, the h_{conv} should be greater than 1300 W/(m^{2}K). Future work will incorporate costs in order to optimise the electrical and thermal performance at the lowest heat sink cost.

Acknowledgement

Marios Theristis acknowledges the financial support of the Royal Society of Edinburgh through the J. M. Lessell's scholarship and the Center for Sustainable Energy Systems, Fraunhofer USA through the research fellowship. The authors would like to thank Pooja Kapadia for her help on the preparation of the TMY3 input files.

References

[1] E. F. Fernández, A. J. G. Loureiro, and G. P. Smestad, "Multijunction Concentrator Solar Cells: Analysis and Fundamentals," in *High Concentrator Photovoltaics*, P.

Pérez-Higueras and E. F. Fernández, Eds., 1 ed: Springer International Publishing, 2015, pp. 9-37.

[2] M. Steiner, A. Bösch, A. Dilger, F. Dimroth, T. Dörsam, M. Muller, T. Hornung, G. Siefer, M. Wiesenfarth, and A. W. Bett, "FLATCON® CPV module with 36.7% efficiency equipped with four-junction solar cells," *Progress in Photovoltaics: Research and Applications*, pp. n/a-n/a, 2014.

[3] Z. Wang, H. Zhang, D. Wen, W. Zhao, and Z. Zhou, "Characterization of the InGaP/InGaAs/Ge triple-junction solar cell with a two-stage dish-style concentration system," *Energy Conversion and Management,* vol. 76, pp. 177-184, 2013.

[4] E. F. Fernández, P. Pérez-Higueras, A. J. Garcia Loureiro, and P. G. Vidal, "Outdoor evaluation of concentrator photovoltaic systems modules from different manufacturers: first results and steps," *Progress in Photovoltaics: Research and Applications,* vol. 21, pp. 693-701, 2013.

[5] B. Marion, "Influence of atmospheric variations on photovoltaic performance and modeling their effects for days with clear skies," in *Photovoltaic Specialists Conference (PVSC), 2012 38th IEEE*, 2012, pp. 003402-003407.

[6] M. Muller, S. Kurtz, M. Steiner, and G. Siefer, "Translating outdoor CPV I–V measurements to a CSTC power rating and the associated uncertainty," *Progress in Photovoltaics: Research and Applications,* pp. n/a-n/a, 2015.

[7] N. Xu, J. Ji, W. Sun, L. Han, H. Chen, and Z. Jin, "Outdoor performance analysis of a 1090× point-focus Fresnel high concentrator photovoltaic/thermal system with triple-junction solar cells," *Energy Conversion and Management*, vol. 100, pp. 191-200, 2015.

[8] K. Nishioka, T. Takamoto, T. Agui, M. Kaneiwa, Y. Uraoka, and T. Fuyuki, "Annual output estimation of concentrator photovoltaic systems using high-efficiency InGaP/InGaAs/Ge triple-junction solar cells based on experimental solar cell's characteristics and field-test meteorological data," *Solar Energy Materials and Solar Cells,* vol. 90, pp. 57-67, Jan 6 2006.

[9] *Suncore Website, http://suncoreus.com/, [Accessed July 27, 2015]*.

[10] *Semprius Website, http://semprius.com/, [Accessed July 27, 2015].*

[11] M. D. Perez and N. E. Gorji, "Modeling of temperature profile, thermal runaway and hot spot in thin film solar cells," *Materials Science in Semiconductor Processing,* vol. 41, pp. 529-534, 2016.

[12] S. Kurtz, M. Muller, D. Jordan, K. Ghosal, B. Fisher, P. Verlinden, J. Hashimoto, and D. Riley, "Key parameters in determining energy generated by CPV modules," *Progress in Photovoltaics: Research and Applications*, pp. n/a-n/a, 2014.

[13] C. Renno, F. Petito, and A. Gatto, "Artificial neural network models for predicting the solar radiation as input of a concentrating photovoltaic system," *Energy Conversion and Management*, vol. 106, pp. 999-1012, 2015.

[14] P. Blumenfeld, J. Foresi, Y. Lang, and J. Nagyvary, "Thermal management and engineering economics in CPV design," in *MEPTEC Symposium Proceedings No. 41*, San Jose, CA, USA, 2011, pp. 206-234.

[15] E. F. Fernández and F. Almonacid, "A new procedure for estimating the cell temperature of a high concentrator photovoltaic grid connected system based on atmospheric parameters," *Energy Conversion and Management*, vol. 103, pp. 1031-1039, 2015.

[16] M. Theristis and T. S. O'Donovan, "Electrical-thermal analysis of III–V triple-junction solar cells under variable spectra and ambient temperatures," *Solar Energy,* vol. 118, pp. 533-546, 2015.

[17] NREL. (2015). *National solar radiation database; Typical meteorological year 3 (TMY3)*. Available: http://rredc.nrel.gov/solar/old_data/nsrdb/1991-2005/tmy3/

[18] ASTM G173-03(2012), Standard Tables for Reference Solar Spectral Irradiances: Direct Normal and Hemispherical on 37° Tilted Surface, ASTM International, West Conshohocken, PA, 2012, www.astm.org

[19] M. Theristis, C. Stark, and T. S. O'Donovan, "Determination of the cooling requirements for single cell photovoltaic receivers under variable atmospheric parameters," in *Photovoltaic Specialist Conference (PVSC), 2015 IEEE 42nd*, 2015, pp. 1-5.

[20] C. A. Gueymard, "Simple Model of the Atmospheric Radiative Transfer of Sunshine, version 2 (SMARTS2): Algorithms description and performance assessment," Florida Solar Energy Center, 1995.

[21] M. Theristis and T. S. O'Donovan, "An integrated thermal electrical model for single cell photovoltaic receivers under concentration," in *15th International Heat Transfer Conference (IHTC-15)*, Kyoto, Japan, 2014, pp. n/a-n/a.

[22] R. Núñez, C. Domínguez, S. Askins, M. Victoria, R. Herrero, I. Antón, and G. Sala, "Determination of spectral variations by means of component cells useful for CPV rating and design," *Progress in Photovoltaics: Research and Applications,* pp. n/a-n/a, 2015.

[23] B. García-Domingo, J. Aguilera, J. de la Casa, and M. Fuentes, "Modelling the influence of atmospheric conditions on the outdoor real performance of a CPV (Concentrated Photovoltaic) module," *Energy,* vol. 70, pp. 239-250, 2014.

[24] G. Nofuentes, B. García-Domingo, J. V. Muñoz, and F. Chenlo, "Analysis of the dependence of the spectral factor of some PV technologies on the solar spectrum distribution," *Applied Energy,* vol. 113, pp. 302-309, 2014.

[25] E. F. Fernández, F. Almonacid, A. Soria-Moya, and J. Terrados, "Experimental analysis of the spectral factor for quantifying the spectral influence on concentrator photovoltaic systems under real operating conditions," *Energy,* 2015.

[26] E. F. Fernández, F. Almonacid, J. A. Ruiz-Arias, and A. Soria-Moya, "Analysis of the spectral variations on the performance of high concentrator photovoltaic modules operating under different real climate conditions," *Solar Energy Materials and Solar Cells,* vol. 127, pp. 179-187, 2014.

[27] J. Hashimoto, S. Kurtz, K. Sakurai, M. Muller, and K. Otani, "Performance of CPV system using three types of III-V multi-junction solar cells," in *CPV-8*, Toledo, Spain, 2012, pp. 372-375.

[28] C. Domínguez, I. Antón, G. Sala, and S. Askins, "Current-matching estimation for multijunction cells within a CPV module by means of component cells," *Progress in Photovoltaics: Research and Applications,* vol. 21, pp. 1478-1488, 2013.

[29] C. Dominguez, S. Askins, I. Anton, and G. Sala, "Characterization of five CPV module technologies with the Helios 3198 solar simulator," in *Photovoltaic Specialists Conference (PVSC), 2009 34th IEEE*, 2009, pp. 001004-001008.

[30] C. Stark and M. Theristis, "The impact of atmospheric parameters on the spectral performance of multiple photovoltaic technologies," in *Photovoltaic Specialist Conference (PVSC), 2015 IEEE 42nd*, 2015, pp. 1-5.

[31] S. P. Philipps, G. Peharz, R. Hoheisel, T. Hornung, N. M. Al-Abbadi, F. Dimroth, and A. W. Bett, "Energy harvesting efficiency of III-V triple-junction concentrator solar cells under realistic spectral conditions," *Solar Energy Materials and Solar Cells,* vol. 94, pp. 869-877, May 2010.

[32] T. Hornung, M. Steiner, and P. Nitz, "Estimation of the influence of Fresnel lens temperature on energy generation of a concentrator photovoltaic system," *Solar Energy Materials and Solar Cells,* vol. 99, pp. 333-338, 2012.

[33] G. S. Kinsey, "Spectrum Sensitivity, Energy Yield, and Revenue Prediction of PV Modules," *Photovoltaics, IEEE Journal of,* vol. 5, pp. 258-262, 2015.

[34] E. F. Fernandez, A. Soria-Moya, F. Almonacid, and J. Aguilera, "Comparative assessment of the spectral impact on the energy yield of high concentrator and conventional photovoltaic technology," *Solar Energy Materials and Solar Cells (in press)*, 2015.

[35] E. F. Fernández, P. Rodrigo, F. Almonacid, and P. Pérez-Higueras, "A method for estimating cell temperature at the maximum power point of a HCPV module under actual operating conditions," *Solar Energy Materials and Solar Cells,* vol. 124, pp. 159-165, 2014.

[36] Spectrolab. (2009, June 10, 2014). *C1MJ concentrator solar cell assembly data sheet (prototype product)*. <*http://www.spectrolab.com/DataSheets/PV/CPV/C1MJ%2009%2018%2009.pdf*>.

[37] G. S. Kinsey and K. M. Edmondson, "Spectral Response and Energy Output of Concentrator Multijunction Solar Cells," *Progress in Photovoltaics,* vol. 17, pp. 279-288, Aug 2009.

[38] S. Senthilarasu, E. F. Fernández, F. Almonacid, and T. K. Mallick, "Effects of spectral coupling on perovskite solar cells under diverse climatic conditions," *Solar Energy Materials and Solar Cells,* vol. 133, pp. 92-98, 2015.

[39] E. F. Fernandez, F. Almonacid Cruz, T. K. Mallick, and S. Sundaram, "Effect of Spectral Irradiance Variations on the Performance of Highly Efficient Environment-Friendly Solar Cells," *Photovoltaics, IEEE Journal of,* vol. 5, pp. 1150-1157, 2015.

[40] F. Almonacid, P. J. Pérez-Higueras, E. F. Fernández, and P. Rodrigo, "Relation between the cell temperature of a HCPV module and atmospheric parameters," *Solar Energy Materials and Solar Cells,* vol. 105, pp. 322-327, 2012.

[41] P. Espinet-González, C. Algora, N. Núñez, V. Orlando, M. Vázquez, J. Bautista, and K. Araki, "Temperature accelerated life test on commercial concentrator III–V triple-junction solar cells and reliability analysis as a function of the operating temperature," *Progress in Photovoltaics: Research and Applications,* vol. 23, pp. 559-569, 2015.

[42] P. Faine, S. R. Kurtz, C. Riordan, and J. M. Olson, "The Influence of Spectral Solar Irradiance Variations on the Performance of Selected Single-Junction and Multijunction Solar-Cells," *Solar Cells,* vol. 31, pp. 259-278, Jun 1991.

[43] I. Mudawar, "Assessment of high-heat-flux thermal management schemes," *Components and Packaging Technologies, IEEE Transactions on,* vol. 24, pp. 122-141, 2001.